WILEY-VCH

DOI: 10.1002/aenm.201802476

Article type: Full Paper

Charge and Triplet Exciton Generation in Neat $PC_{70}BM$ Films and Hybrid CuSCN:$PC_{70}BM$ Solar Cells

Safakath Karuthedath[1], Julien Gorenflot[1], Yuliar Firdaus[1], Wai-Yu Sit[2], Flurin Eisner[2], Akmaral Seitkhan[1], Mahesh Kumar Ravva[1,3], Thomas D. Anthopoulos[1,2], Frédéric Laquai[1*]*

Dr. S. Karuthedath, Dr. J. Gorenflot, Dr. Y. Firdaus, A. Seitkhan, Dr. M. K.Ravva, Prof. T. D. Anthopoulos, Assoc. Prof. F. Laquai

King Abdullah University of Science and Technology (KAUST), KAUST Solar Center (KSC), Physical Sciences and Engineering Division (PSE), Material Science and Engineering Program (MSE), Thuwal 23955-6900, Kingdom of Saudi Arabia.

Emails: safakath.karuthedath@kaust.edu.sa, frederic.laquai@kaust.edu.sa

W. Sit, F. Eisner, Prof. T. D. Anthopoulos

Department of Physics, Imperial College London, South Kensington, London SW7 2AZ, United Kingdom

Dr. M. K.Ravva

Department of Chemistry, SRM University-AP, Amaravati-522502, India.

Keywords: fullerene; hybrid solar cells; copper thiocyanate; triplet exciton; transient absorption spectroscopy

The authors S.K and J. G contributed equally to this work.

Abstract

Organic solar cells that use only fullerenes as photoactive material exhibit poor exciton-to-charge conversion efficiencies, resulting in low internal quantum efficiencies (IQE). However, the IQE can be greatly improved, when copper(I)thiocyanate (CuSCN) is used as a carrier-selective interlayer between the $PC_{70}BM$ (phenyl-C70-butyric acid methyl ester layer) and the anode. Efficiencies of ~5.4% have recently been reported for optimized CuSCN:$PC_{70}BM$ (1:3) mesostructured heterojunctions, yet the reasons causing the efficiency boost remained unclear. Here, transient absorption (TA) spectroscopy is used to demonstrate that CuSCN does not only act as a carrier-selective electrode layer, but also facilitates fullerene exciton dissociation and hole transfer at the interface with $PC_{70}BM$. While intrinsic charge generation in neat $PC_{70}BM$ films proceeds with low yield, hybrid films exhibit much improved exciton dissociation due to the presence of abundant interface. Triplet generation with a rate proportional to the product of singlet and charge concentrations is observed in neat $PC_{70}BM$ films, implying a charge–singlet spin exchange mechanism, while in hybrid films this mechanism is absent and triplet formation is a consequence of non-geminate recombination of free charges. At low carrier concentrations, the fraction of charges outweighs the population of triplets, leading to respectable device efficiencies under one sun illumination.

1. Introduction

Fullerene derivatives are ubiquitous electron acceptor and transport materials in organic photovoltaic (OPV) devices due to their large electron affinity and ability to form both finely-intermixed blends as well as aggregates, identified as important for charge separation, when blended with an electron donor material.[1] Although fullerenes have been used widely in OPV devices, their (photo)excited state properties have received relatively little attention up to now.[2-6] However, the role of fullerenes as light absorber contributing to the photocurrent generation has gained increasing recognition as several recent reports demonstrate.[2, 7-10] In fact, these studies suggest that fullerenes not only play a role as electron acceptor, but also can contribute significantly to light harvesting in the photoactive layer.[2, 3, 6-8, 11] For instance, Burkhard et al. showed that free charge carriers can be generated upon light absorption by fullerenes.[9] Keiderling et al. reported charge carrier generation from charge transfer (CT) excitons in neat $PC_{60}BM$ films.[3] In contrast, Chow et al. reported that the photoexcited states of $PC_{70}BM$ films consist of singlet and triplet excitons, while no evidence for intrinsic charge generation was observed.[4] Due to the high electron-hole (exciton) binding energy neat fullerene solar cells exhibit very low external quantum efficiency (EQE).[9] However, recently it has been shown that blending fullerene molecules with optically transparent high bandgap inorganic compounds in a hybrid heterointerface improves substantially the power conversion efficiencies of such cells.[12] In fact, a recent report by Sit et al. showed that, when copper(I)thiocyanate (CuSCN) was blended with $PC_{70}BM$, a more than fivefold increase in power conversion efficiency (PCE) could be achieved in single junction solar cells using $PC_{70}BM$ as the only light absorber.[12] Subsequently, Firdaus et al. demonstrated that the substantial increase in PCE in hybrid $PC_{70}BM$:CuSCN solar cells is caused by improved charge carrier generation and transport, facilitated by the unique meso-structure of CuSCN nanowires penetrating the $PC_{70}BM$ domain.[13]

Here, we study the photophysics of neat $PC_{70}BM$ films and compare them to CuSCN:$PC_{70}BM$ blends to understand what determines the efficiency of such devices. Using picosecond (ps) to microsecond transient absorption (TA) spectroscopy and multivariate curve resolution (MCR) analysis, we find that in neat $PC_{70}BM$ films, charge carriers are generated from singlet excitons over tens of ps. Interestingly, only if charge carriers and singlet states are present at the same time, triplet excitons are generated in neat fullerene films. Hence, we propose that triplets are formed by singlet-charge spin exchange and not by intersystem crossing (ISC) from singlet states. This is in stark contrast to previous reports that assigned triplet generation in neat fullerenes to intersystem crossing from singlet excitons.[3-5] In contrast, in blends with CuSCN ultrafast generation of charge carriers is observed due to the abundance of donor/acceptor (D/A) interface, while triplet state formation is slow and a consequence of non-geminate recombination of free charge carriers. We find that the fraction of charge carriers outweighs largely the population of triplet excitons in both, blends and neat films.

2. Result and Discussion

2.1. Steady-State Device Characterization

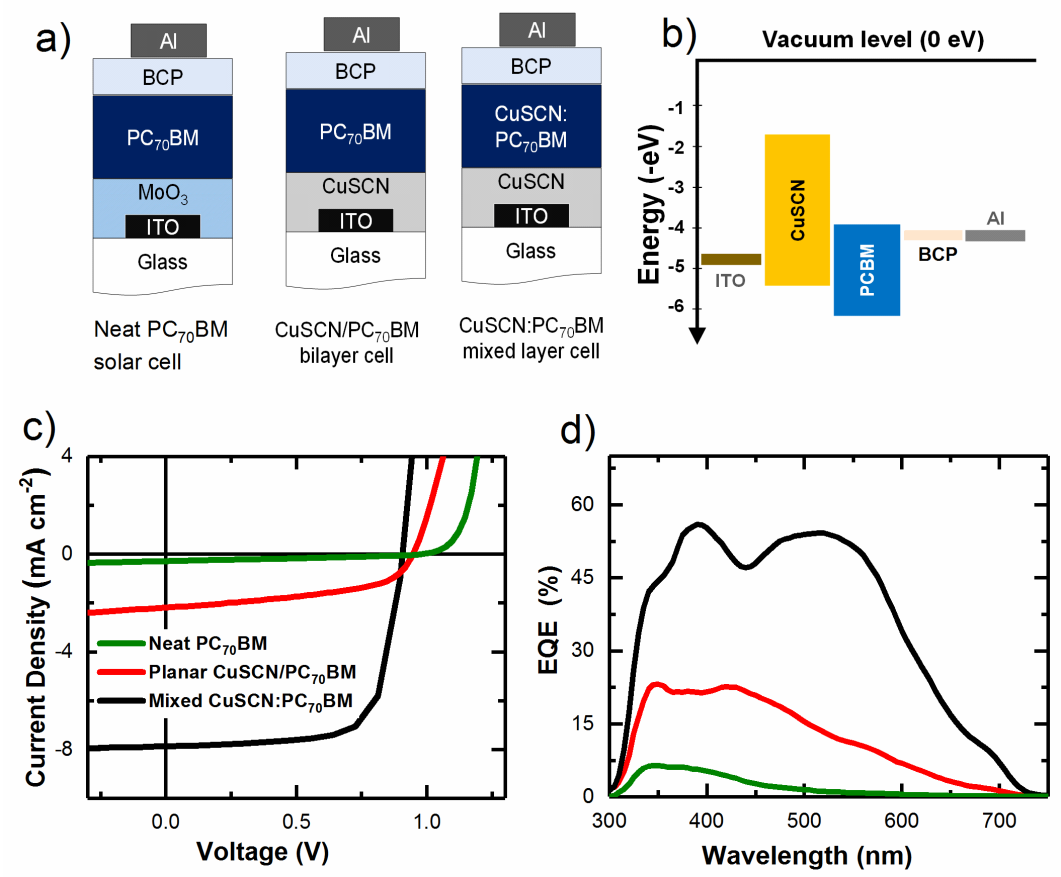

Figure 1: (a) Device structures of the solar cells used in this study. (b) Energy level diagram of the devices. (c) Current density-voltage (J-V) characteristics of neat $PC_{70}BM$ (green), bilayer CuSCN/$PC_{70}BM$ (red), and mixed CuSCN:$PC_{70}BM$ (black) solar cells and (d) their corresponding external quantum efficiencies.

Figure 1a shows the device structures of neat $PC_{70}BM$, bilayer CuSCN/$PC_{70}BM$, and hybrid mesostructured CuSCN:$PC_{70}BM$ heterojunction solar cells, while Figure 1b depicts the energetics of each layer in the device. Details of the device fabrication can be found in the Experimental Section. Figure 1c and 1d show the current-voltage (*J-V*) curve and external quantum efficiency (*EQE*) spectra, respectively, of neat $PC_{70}BM$ films (MoO_3 as hole transport layer, green curves), exhibiting a PCE <0.1% with a maximum external quantum efficiency (EQE) around 7% at 340 nm. Corresponding UV-Vis absorption spectra are shown in Figure S1. Despite the poor performance, the photocurrent generation in neat films indicates free charge carrier generation in line with previous reports.[2, 6, 8, 9] Furthermore, optimized CuSCN/$PC_{70}BM$ bilayer devices ($PC_{70}BM$ thickness: 40 nm) showed a PCE of more than 1 %, while optimized CuSCN:$PC_{70}BM$ blends yielded a PCE of 5.4 % (see red and black curves in

Figure 1). In line with the PCE, the EQE increased by a factor of three in bilayer CuSCN/$PC_{70}BM$ solar cells (Figure 1d, red curve) compared to neat $PC_{70}BM$ cells, and further improved by a factor of 2.5 when changing from a bilayer hybrid solar cell to the hybrid blend system (Figure 1d, black curve), in line with recent reports.[2, 13] To understand this remarkable improvement in short circuit current density (J_{SC}) and PCE, we employed picosecond-microsecond transient absorption spectroscopy on neat fullerene films and on CuSCN:$PC_{70}BM$ blends.

2.2. Transient Absorption Spectroscopy on Neat $PC_{70}BM$ Films

Transient absorption spectra were measured with a homebuilt setup across a time window from ~300 fs to ~300 µs with a spectral coverage from ~0.85 eV to ~3.2 eV.[14] A detailed experimental description can be found in the Supporting Information. **Figure 2**a shows the picosecond-nanosecond TA spectra of a neat $PC_{70}BM$ film measured under vacuum after excitation at 370 nm with ~100 fs pulses. The ground state bleach (GSB), observed as positive spectral feature from 2.0 – 3.0 eV, and photo-induced absorption (PA), i.e., the negative spectral region below 2.0 eV, show comparable temporal evolution, whereas the structured (multiple peaks) PA centered at 1.8 eV decays significantly faster. The signal in the low energy spectral region (1.1-1.2 eV) decays slowly and evolves into a flat PA, while the high-energy part shows a faster decay (see also Figure S2). Figure 2b represents the spectrally-integrated (1.5-1.9 eV) TA kinetics of pristine $PC_{70}BM$ films for a range of fluences. The spectral evolution (Figure 2a) indicates that after photogeneration of singlet excitons, formation of different states such as triplets and/or charges occurs on this timescale and the fluence dependence of the dynamics points to subsequent reactions between these states. However, we cannot entirely rule out that singlet-singlet annihilation (SSA) contributes to some extent to the observed fluence dependence.

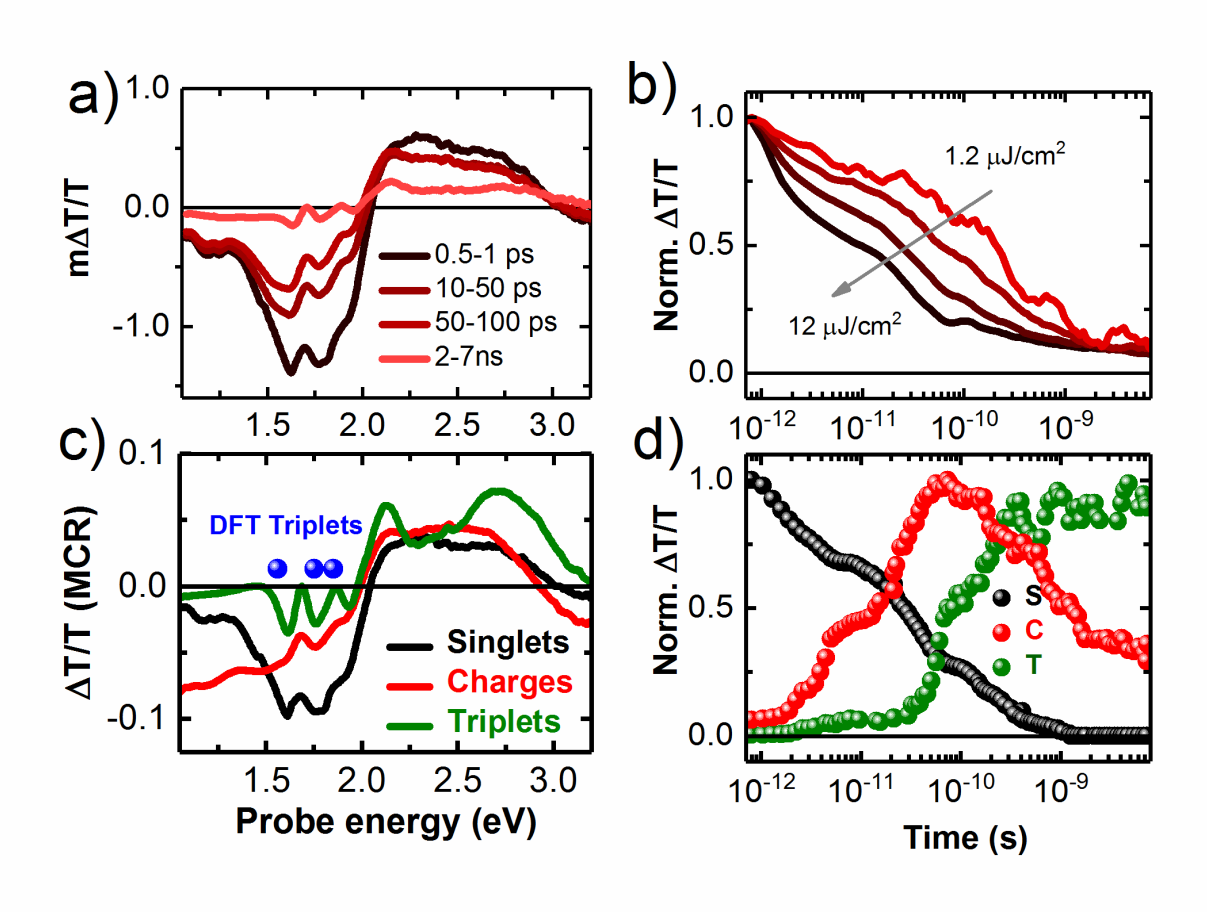

Figure 2: TA on pristine $PC_{70}BM$ film. (a) ps-ns TA spectra of a neat $PC_{70}BM$ film measured under vacuum and (b) the spectrally-integrated dynamics in the region from 1.5 eV - 1.9 eV for a wide range of fluences. Panel (c) shows the component spectra obtained by MCR analysis and panel (d) shows the corresponding kinetics for ps-ns TA at 3.5 μJ/cm^2 extracted from MCR. Blue symbols in panel (c) indicate the calculated spectral positions of triplet state absorption obtained by Time Dependent-Density Functional Theory (TD-DFT).

The superposition of features from various excited states makes kinetic analysis challenging. To address this issue and gain more insight into the nature of the excited states and their dynamics, we employed multivariate curve resolution (MCR) on the experimentally-measured TA data matrix. MCR is a soft modelling technique introduced by Jaumot et al. and previously used by us and others to deconvolute complex transient absorption spectra into separate components.[15, 16] Figure 2c shows the spectra of different components found in pristine $PC_{70}BM$ films by MCR analysis. We note that using only two components in the MCR analysis did not result in a satisfactory description of the experimental TA data, while three components yielded a satisfactory description (see Figure S3a for a comparison of two component vs. three component MCR analysis). Based on a comparison of the MCR component spectra with

literature spectra, we assign the three components as follows: firstly, the spectrum peaking at 1.6-1.9 eV is assigned to singlet exciton-induced absorption, as it is very similar to the TA spectra at 0.5 ps (black line, panel a) and also in line with the spectrum reported earlier for $PC_{70}BM$ singlets.[4] Secondly, The broad PA band extending from 1.1-2.0 eV and even further into the low energy spectral region and is assigned to charge-induced absorption. MCR shows (panel c, red curve) that $PC_{70}BM$ charge carriers (both anions and cations) absorb broadly across the entire PA region of the $PC_{70}BM$ spectrum, in line with earlier reports.[17-19] Thirdly, the spectrum that exhibits multiple peaks at 1.94 eV, 1.77 eV, 1.61 eV, and at 1.25 eV, is assigned to triplet states, which is in line with a previous report.[4] Note that the band at 1.25 eV is very weak and that this spectral region is dominated by charge-induced absorption. The calculated lowest three triplet absorption energies of a $PC_{70}BM$ molecule via time dependent density functional theory (TD-DFT) are 1.56 eV, 1.75 eV, and 1.84 eV, which supports our assignment of the spectral features obtained by MCR analysis to $PC_{70}BM$ triplet states. Additionally, our MCR results show that the charge-induced absorption signal rises to 20 % of the amplitude of the exciton-induced absorption signal in neat $PC_{70}BM$ films (Figure S3). The observation of charge generation in neat $PC_{70}BM$ films is in contrast to a previous report from Chow et al., who assigned the TA signals of $PC_{70}BM$ to singlet and triplet excitons only.[4] However, we note that in line with our observation, the Durrant group recently reported evidence of charge generation in neat $PC_{60}BM$ films observed by transient absorption spectroscopy[3], in accordance with previous reports on free charge generation from loosely-bound intramolecular excitons generated from high energy photons.[20] In fact, the observation of charges in pristine $PC_{70}BM$ films explains why $PC_{70}BM$-only devices generate a photocurrent as recently reported by the Anthopoulos group (also see Figure 1).[12, 13] However, the exciton-to-charge conversion efficiency is low and thus the PCE of neat fullerene solar cells remains also low. The low photocurrent of neat $PC_{70}BM$ devices is consistent with the low

density of charge carriers compared to the density of photogenerated singlet excitons (see also Figure S3b for non-normalized MCR kinetics).

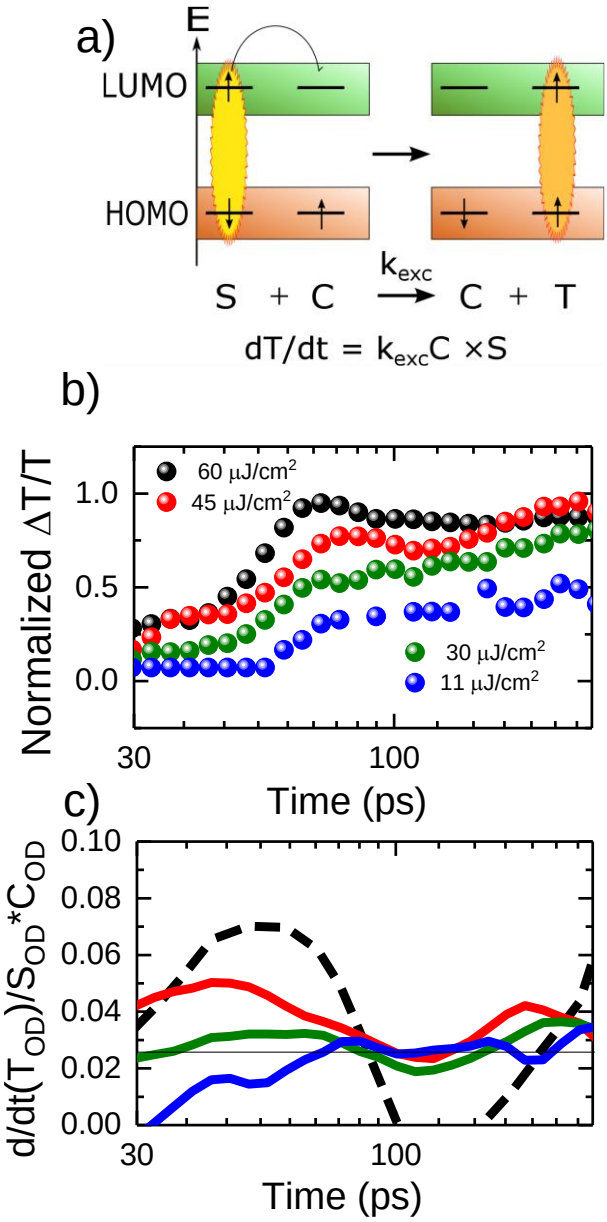

Figure 3: (a) Schematic representation of singlet-charge spin exchange, associated rate equation and triplet formation rate. (b) Fluence dependent evolution of the triplet population obtained from MCR. (c) Ratio of the triplet signal amplitude divided by the product of the singlet and charge-induced signal amplitude as extracted by MCR for the temporal region, in which all three states are observed.

We now discuss the kinetics of all three components obtained by MCR analysis for an excitation fluence of 3.5 μJ/cm^2 (Figure 2d). Singlet excitons (black symbols) decay mostly within ~500 ps, while the charge carrier population rises until ~70-100 ps. On the same time scale, roughly

starting at 30 ps, that is when charge carriers and singlets are both present at the same time, the triplet population (green symbols) increases and it keeps rising up to 1 ns as also reported by others.[4] Interestingly, triplet excitons are only generated in neat $PC_{70}BM$ films when both charge carriers and singlet excitons are present at the same time. Thus, we hypothesize that triplets are created by singlet-charge spin exchange and not by intersystem crossing (see **Figure 3**) in $PC_{70}BM$. This is in contrast to previous reports that concluded triplet generation in neat fullerenes is a consequence of intersystem crossing (ISC) from singlet excitons.[3-5] However, the decay of singlet excitons – too fast for efficient ISC – and the delayed generation of triplet excitons (up to 40 ps) observed here implies that the mechanism of triplet generation is not ISC, which is typically observed on a nanosecond time scale.[3] Notably, triplet generation does neither occur before charges are present, nor if only singlets states are present, which excludes singlet-singlet annihilation (SSA) as origin of triplet formation. Moreover, triplet generation does not occur after singlet excitons have disappeared, indicating they participate in the triplet formation reaction and thus excluding that they are generated by free charge recombination. In particular, during the decay of the charge-induced absorption signal no further rise of the triplet signal is observed (see Figure 2d). Hence, we hypothesize a triplet formation mechanism as exemplified for a positive charge carrier (hole) in Figure 3a. For such an elementary mechanism, we expect the reaction rate to be proportional to the product of the densities of singlet excitons and charges. In fact, this is what we observe: the triplet formation rate (expressed by dT_{OD}/dt) divided by the product of the singlet and charge carrier signals (S_{OD} and C_{OD}) is found to be rather constant (around 0.025) during the triplet generation at the three lowest fluences. We note that a meaningful derivation is only possible for the time range where all three signals, that is, S_{OD}, C_{OD}, and T_{OD} are sufficiently large and provide an acceptable signal-to-noise ratio (see Figures 3b and 3c). However, for the highest fluence this model appears not to entirely capture the dynamics of the triplet-induced absorption signal, likely due

to the onset of singlet-singlet annihilation (faster raise prior to 80 ps) or triplet–triplet annihilation (early decay from ~80 ps onwards).

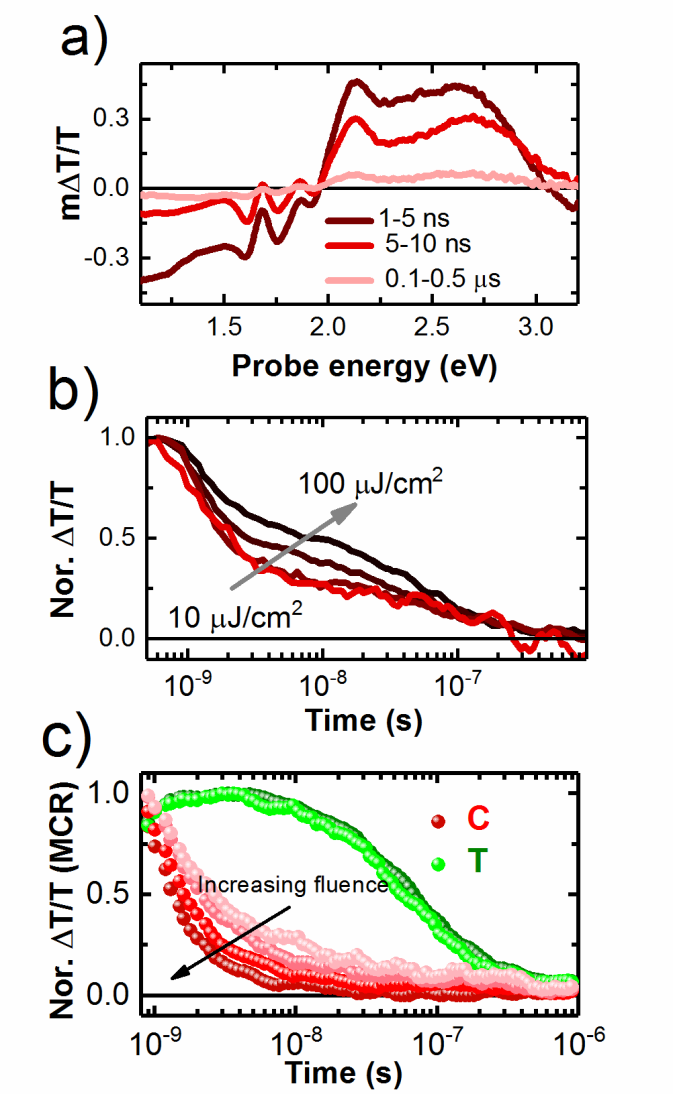

Figure 4: Nanosecond-microsecond TA on a pristine $PC_{70}BM$ film. (a) Spectra measured at different delay times under vacuum and (b) the spectrally-integrated kinetics of the 1.5 eV-2 eV spectral region. Panel (c) shows the deconvoluted kinetics of triplets (green) and charge carriers (red) obtained from MCR analysis of the ns-µs TA data.

We now turn to the ns - µs spectra and dynamics. **Figure 4**a shows TA spectra of a neat $PC_{70}BM$ film. On the ns - µs time scale, three bands positioned at 1.93 eV, 1.77 eV, and 1.64 eV, respectively, emerge along with another band at 1.25 eV. They resemble the triplet exciton absorption as reported earlier by Chow et al.[4] However, the low energy band centered at 1.25 eV exhibits a slower decay than the other peaks on the ns - µs timescale and prevails at long

delay times, indicating that it originates from a different excited state (Figure S6). We assign this band to $PC_{70}BM$ anions, in agreement with existing literature reports.[17, 19]

Unlike the ps-ns spectra, the absorption band at 1.25 eV has more spectral weight compared to the other PA band due to the presence of long-lived charge carriers. We also measured ns-µs TA in air and found that the 1.25 eV band decays slower than the 1.5 eV-2.0 eV region, which is typically the case for charge carriers (Figure S5).[3, 21, 22] In the region of charge-induced absorption (1.25 eV), more than 90% of the signal (at 1.25 eV) decays within 500 ns. This decay is faster at higher fluences, indicating that separated charge carriers undergo non-geminate recombination (Figure S6, panel a). In contrast, in the 1.5-2.0 eV spectral region where both charge and triplet signals are expected, the integrated kinetics (Figure 4b) show a slower decay at higher fluences. This is surprising and we assign it to the larger fraction of long-live triplet excitons observed at higher fluences in this spectral region. In fact, at higher fluences, long-lived triplet excitons dominate the kinetics, whereas at lower fluences, the fraction of triplet excitons is very low as confirmed by MCR analysis (vide infra). The spectral evolution suggest that there are at least two components present on this time scale. Hence, we employed MCR analysis to separate the components on the nanosecond-microsecond timescale.

Figure 4c shows the kinetics traces of charges and triplets as obtained by MCR analysis, showing that the triplet excitons persist longer than the charge carriers do. The fluence independent decay of the triplet exciton signal proves the absence of charge-triplet annihilation. We note that, at lower fluences the triplet exciton density is very low, suggesting that at low fluence the triplet generation via the singlet-charge spin exchange mechanism is less pronounced, as the density of singlets and charges are too low for singlet-charge encounter to occur with a non-negligible probability. In contrast, the charge carriers show fluence dependent non-geminate recombination dynamics. This clarifies the incongruity in the decay of the 1.5-2 eV spectral region: at low fluence most of the signal is from charges, because triplet generation is not efficient and charges recombine faster than triplets. We note that, at very low fluence the

charge carrier contribution outweighs that of triplets, as the triplet generation is fluence dependent (see Figure S7 for non-normalized MCR kinetics). Extrapolating to carrier densities in a device under solar condition, where the charge density is significantly lower than studied here (~10-100 times lower), we expect a negligible build-up of triplet excitons. These results together with other recent studies[3, 9, 12] suggest that fullerene and its derivatives are capable of producing substantial photocurrent and this needs to be taken into account when discussing the device physics of fullerene-based solar cells.

2.3. Transient Absorption Spectroscopy on Hybrid CuSCN:$PC_{70}BM$ Blend Films

Having established the nature of charge and triplet exciton generation in neat $PC_{70}BM$ films, we now turn to examining the nature of charge generation at the hybrid CuSCN/$PC_{70}BM$ interface. This interface is one of few hybrid interfaces, which have been reported to facilitate charge generation.[12, 13] **Figure 5**a shows the ps-ns TA spectra of thin-film CuSCN:$PC_{70}BM$ blends (1:3) measured in vacuum. The band at 0.93 eV (1330 nm) is assigned to $PC_{70}BM$ anions in line with previous reports.[17, 19] The band at 1.25 eV is composed of both $PC_{70}BM$ charge and triplet exciton absorption as observed for the neat film (vide supra) and confirmed by MCR analysis (vide infra). Figure 5b represents the ps-ns spectrally-integrated dynamics (1.5-1.9 eV) of the blend. As is the case for neat films, a fluence-dependent decay is observed, however, slower compared to neat $PC_{70}BM$ films, suggesting a larger contribution from long-lived species such as charges or triplets and likely to be related to the higher photovoltaic performances of the blend. This notable difference in the excited state dynamics compared to neat $PC_{70}BM$ films suggests that blending $PC_{70}BM$ with CuSCN facilitates hole transfer from $PC_{70}BM$ to CuSCN, which are then transported and collected at the electrodes.

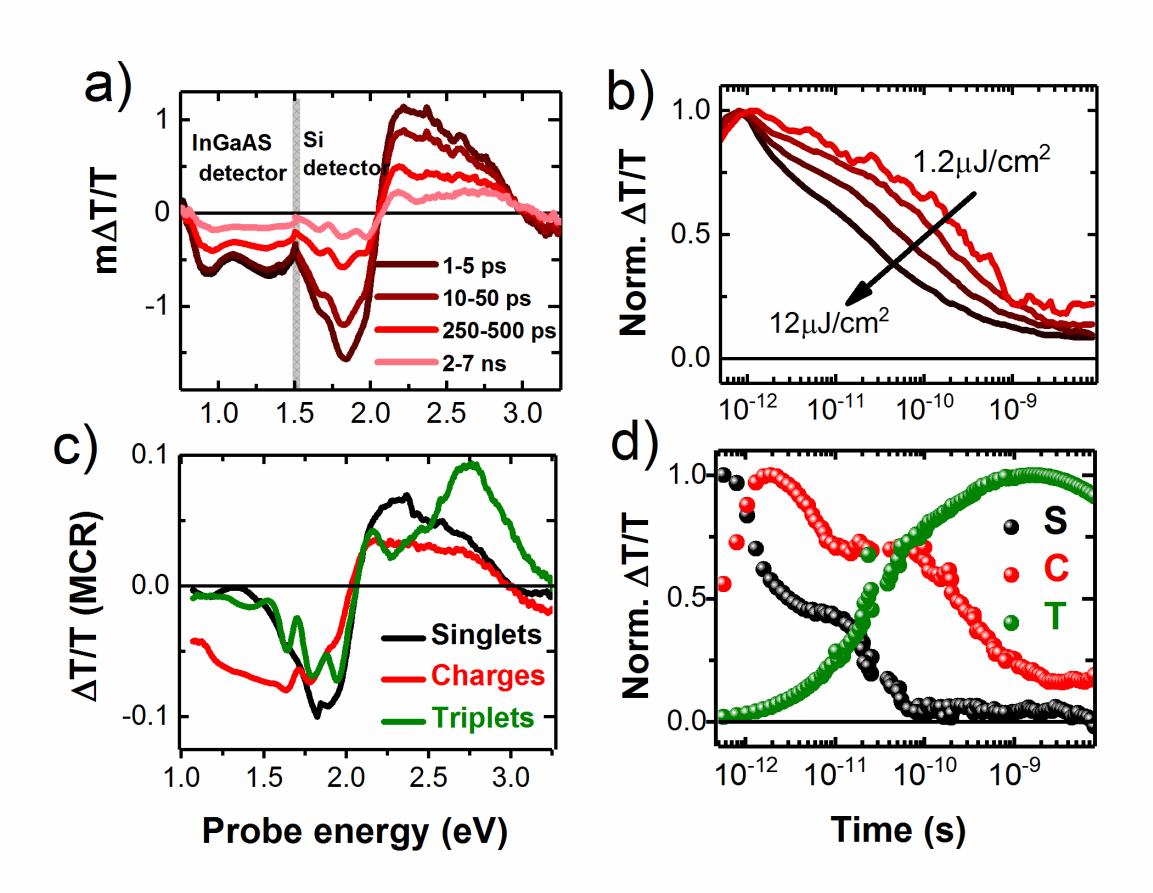

Figure 5: (a) Picosecond-nanosecond TA of a hybrid CuSCN:$PC_{70}BM$ blend film measured under vacuum. The low energy region (<1.5 eV) of the spectrum was measured with an InGaAs detector, while the region above 1.5 eV was measured with a silicon-based detector. (b) Kinetics integrated over the spectral region 1.5 eV-1.9 eV for a wide range of fluences. Panel (c) shows the results of MCR analysis of the TA spectra and panel (d) shows the corresponding kinetics for ps-ns TA at 3.5 μJ/cm^2 determined by MCR.

Figure 5c shows the MCR spectra of the CuSCN:$PC_{70}BM$ blend. The spectra exhibit noticeable differences compared to those of neat $PC_{70}BM$. The charge-induced absorption band is broadened and blue-shifted, while the singlet-induced absorption band is narrower. We hypothesize that in neat films we observe both cations and anions, whereas in the blend we see only $PC_{70}BM$ anions as the holes are extracted to the CuSCN phase. The triplet-induced absorption spectrum is slightly blue shifted compared to that of the neat film. Unlike in the neat film, triplet formation in the blend originates from non-geminate charge carrier recombination, as most of the singlet excitons are quickly converted into charges on the sub-ps time scale (Figure 5d). We explain this by the abundant presence of interface in the blend as morphological studies showed a clear component separation accompanied by a spontaneous formation of

CuSCN nanowire-like crystallites that penetrate into the $PC_{70}BM$ domains in the CuSCN:$PC_{70}BM$ blend layer (see Figure S8 for TEM images).[12] We note that the singlet excitons decay entirely within ~50 ps, more than one order of magnitude faster than observed for neat $PC_{70}BM$ films. Thus, blending of CuSCN with $PC_{70}BM$ leads to efficient quenching of singlet excitons and ultrafast charge carrier generation. Our results suggest that in these hybrid mesostructured heterointerface devices most of the charge carriers are generated within ~1 ps, whereas in the neat fullerene films charge generation is delayed and much less efficient. In contrast to neat fullerene films, triplets in blends are generated by recombination of free charge carriers. In fact, the triplet generation dynamics clearly follows the decay of charges (panel d), suggesting that charge recombination is the origin of triplet generation and dominates over ISC and singlet-charge spin exchange, as on this timescale singlets are not present anymore. This is favorable for device performance, as free charge carriers can be extracted at the electrodes prior to recombination and triplet formation, whereas in neat films, triplet generation competes with charge generation.

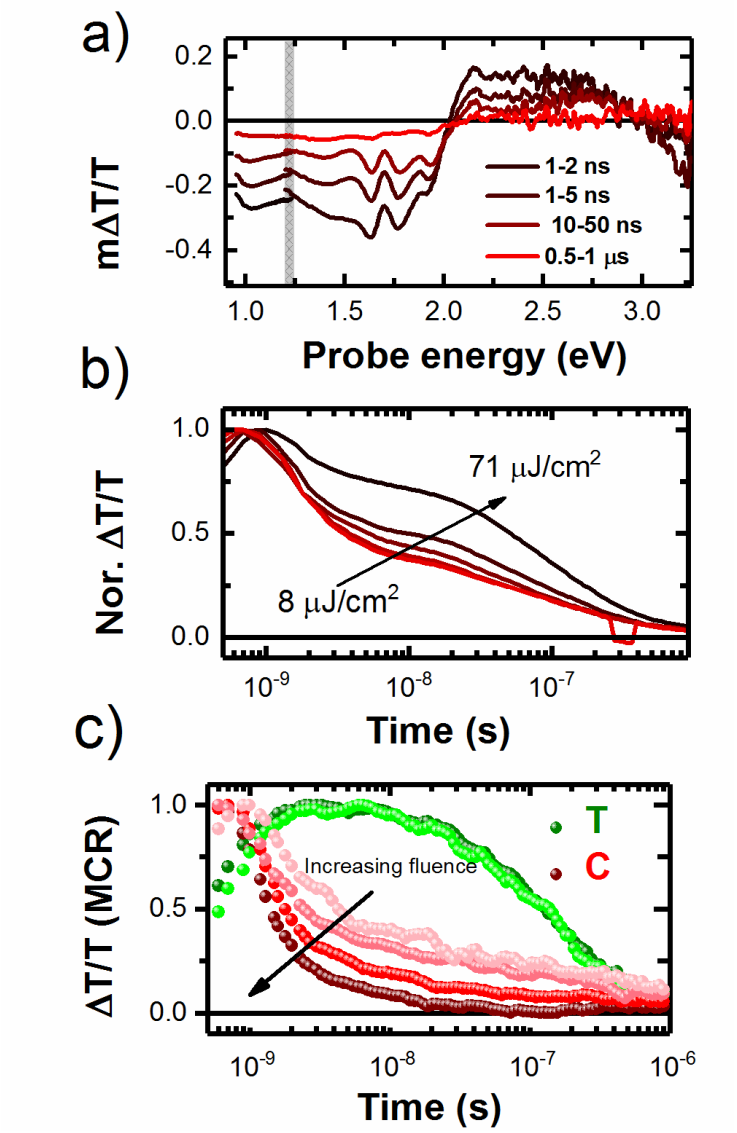

Figure 6: (a) Nanosecond-microsecond TA of a hybrid CuSCN:$PC_{70}BM$ film measured under vacuum. The low energy region (<1.25 eV) of the spectrum was measured with an InGaAs detector, while the region above 1.25 eV was measured with a silicon-based detector. (b) Kinetics integrated over the spectral region 1.5 eV-2 eV for a wide range of fluences. Panel (c) shows the kinetics of triplets (green) and charge carriers (red) obtained from MCR analysis of the ns-μs TA.

Figure 6a shows the ns-μs TA spectra of the blend, illustrating the presence of long-lived states that persist up to several hundreds of nanoseconds and Figure 6b represents the ns-μs decay kinetics of the 1.5-2 eV signal. The recombination is fast compared to that observed in typical polymer:fullerene blends due to the higher electron mobility in the fullerene.[15, 19, 21, 23] Strikingly, as in the case of neat films, kinetic traces of the 1.5-2 eV spectral region show contrasting fluence dependence compared to the low energy band. The integrated kinetics of the 1.15-1.25 eV and 1.5 eV-2 eV spectral regions are shown for comparison in Figure S9.

Figure 6c shows the kinetics of charge carriers and triplets obtained by MCR analysis of the ns-µs TA data. We note that at lower fluences the charge contribution outweighs that of triplet states in the blend as is also observed for neat films (Figure S10). This implies that under solar illumination conditions (low carrier concentration) triplet formation via charge recombination is largely reduced.

3. Conclusion

In conclusion, we observed charge carrier and triplet exciton formation in neat $PC_{70}BM$ films after generation of primary photoexcitations, that are, singlet excitons. We conclude that triplet generation in neat fullerenes is a consequence of singlet-charge spin exchange rather than intersystem crossing, in contrast to earlier reports. In solar cells using neat $PC_{70}BM$ as photoactive layer, the singlet-to-charge conversion efficiency is very low and causes low device EQEs and photocurrents. Incorporating CuSCN as a carrier-selective p-type interlayer (hole extraction layer), a hybrid organic/inorganic interface is created, which facilitates ultrafast and efficient fullerene exciton dissociation and hole extraction. By further examining the transient absorption signal, we deduced that this interface promotes efficient charge carrier separation and extraction of carriers at the electrodes by slowing down the recombination of charges in the photoactive layer. Triplet generation in neat films of $PC_{70}BM$ and CuSCN:$PC_{70}BM$ blends is fluence depdendent, indicating that at solar illumination equivalent to low concentrations of photogenerated states, triplet formation is negligible. We conclude that fullerenes can contribute significantly to photocurrent generation in organic solar cells and matching them with p-type materials can lead to efficient exciton dissociation, charge photogeneration, and photocurrent extraction in hybrid bulk heterojunction solar cells.

4. Experimental Section

Solar Cell Fabrication: Indium tin oxide (ITO) coated glass substrates (Kintec Company, 10 Ω/sq.) were cleaned by sequential ultra-sonication in dilute Extran 300 detergent solution, deionized water, acetone and isopropyl alcohol for 20 minutes each. These substrates were then cleaned by UV-ozone treatment for 20 minutes. Copper (I) thiocyanate (CuSCN) (25 mg/ml) (Sigma-Aldrich) was dissolved in diethyl sulfide (DES) (Sigma-Aldrich) at 60ºC for 1 hour. Such CuSCN solution was then spin-casted at 2500 rpm for 30 s, followed by annealing of the device at 105ºC for 10 minutes.[12, 13]

For the MoO_3/$PC_{70}BM$ cells (neat $PC_{70}BM$ device), a thin layer (~16 nm) of MoO_3 was deposited by thermal evaporation under high vacuum (5×10^{-6} mbar). For bilayer (CuSCN/$PC_{70}BM$) devices, 25 mg/ml of CuSCN solution was spin-casted at 2500 rpm for 30 s, followed by annealing of the device at 105ºC for 10 minutes. The MoO_3-coated and CuSCN-coated substrates were then transferred into a dry nitrogen glove box (< 3 ppm O2). A $PC_{70}BM$ layer (20 mg/ml in chlorobenzene) was spun at 2000 rpm for 30 s (active-layer thickness 30-40 nm). A layer of 10 nm bathocuproine (BCP) (Sigma-Aldrich) followed by a 100 nm of aluminum were then thermally evaporated at 5×10^{-6} mbar to complete the device fabrication.

For thin film composites, a blend of CuSCN:$PC_{70}BM$ was prepared by mixing 15 µL of CuSCN (40 mg/mL in DES) with 45 µL of $PC_{70}BM$ (40 mg/ml in CB) 5 minutes prior to spin-coating (yielding a weight ratio of 1:3). The mixture was then spin-coated at 2000 rpm for 30 s, followed by thermal annealing at 105ºC for 10 minutes. After spin-coating and annealing, all substrates were transferred to a vacuum evaporation chamber for electrode deposition. A layer of 10 nm bathocuproine (BCP) (Sigma-Aldrich) and 100 nm of aluminum were then thermally evaporated at 5×10^{-6} mbar.

Sample Preparation for Spectroscopy: CuSCN:$PC_{70}BM$ blend films and pristine $PC_{70}BM$ films were prepared by spin-coating at a spin speed of 2000 rpm for 30 s from chlorobenzene solution (same conditions as used to prepare the active layer of optimized solar cell devices) onto pre-

cleaned quartz substrates. All substrates were cleaned by sonication for 20 minutes in Extran 300 detergent solution, deionized water, acetone, 2-isopropanol, and UV-ozone treatment.

J-V and EQE Spectra: J-V curves were recorded with a Keithley 2400 Source Meter under AM 1.5G illumination (100 mW cm^{-2}), generated by a solar simulator with a 180 Watt xenon arc lamp as the light source (Model SS50A, Photo Emission Tech., Inc.). The irradiance was set to 1 sun using a standard silicon photodiode calibrated at the Energy Research Centre of the Netherlands (ECN). *EQE* spectra were recorded with a home-built setup using a Newport Merlin lock-in amplifier. Devices were illuminated with chopped monochromatic light through the transparent ITO electrode.

TA Spectroscopy: Transient absorption (TA) spectroscopy was carried out using a home-built pump-probe setup. Two different configurations of the setup were used for either short delay, namely 100 fs to 8 ns experiments, or long delay, namely 1 ns to 100 μs delays, as described below: The output of titanium:sapphire amplifier (Coherent LEGEND DUO, 4.5 mJ, 3 kHz, 100 fs) was split into three beams (2 mJ, 1 mJ, and 1.5 mJ). Two of them were used to separately pump two optical parametric amplifiers (OPA) (Light Conversion TOPAS Prime). The TOPAS 1 generates tunable 700 pump pulses, subsequently frequency doubled to 350 nm with a 2mm thick BBO crystal, while the TOPAS 2 generates signal (1300 nm) and idler (2000 nm) only. A fraction of the output signal of titanium:sapphire amplifier was focused into a c-cut 3 mm thick sapphire window, thereby generating a white-light supercontinuum from 500 to 1600 nm. For short delay TA measurements, we used the TOPAS 1 for producing pump pulses while the probe pathway length to the sample was kept constant at approximately 5 meters between the output of the TOPAS1 and the sample. The pump pathway length was varied between 5.12 and 2.6 m with a broadband retroreflector mounted on automated mechanical delay stage (Newport linear stage IMS600CCHA controlled by a Newport XPS motion controller), thereby generating delays between pump and probe from -400 ps to 8 ns. For measuring TA whole visible range, we used 1300 nm (signal) of TOPAS 2 to produce white-light super continuum

from 350 to 1100 nm. For the 1 ns to 300 μs delay (long delay) TA measurement, the same probe white-light supercontinuum was used as for the 100 fs to 8 ns delays. But the excitation light (pump pulse) was provided by an actively Q-switched Nd:YVO4 laser (INNOLAS picolo AOT) frequency-doubled to provide pulses at 532 nm. The pump laser was triggered by an electronic delay generator (Stanford Research Systems DG535), itself triggered by the TTL sync from the Legend DUO, allowing control of the delay between pump and probe with a jitter of roughly 100 ps. Pump and probe beams were focused on the sample which was kept under a dynamic vacuum of $<10^{-5}$ mbar. The transmitted fraction of the white light was guided to a custom-made prism spectrograph (Entwicklungsbüro Stresing) where it was dispersed by a prism onto a 512 pixel NMOS linear image sensor (HAMAMATSU S8381-512) for Si detector and a 512 pixel CMOS linear image sensor (HAMAMATSU G11608-512DA) for InGaAs detector. The probe pulse repetition rate was 3 kHz, while the excitation pulses were mechanically chopped to 1.5 kHz (100 fs to 8 ns delays) or directly generated at 1.5 kHz frequency (1 ns to 300 μs delays), while the detector array was read out at 3 kHz. Adjacent diode readings corresponding to the transmission of the sample after excitation and in the absence of an excitation pulse were used to calculate $\Delta T/T$. Measurements were averaged over several thousand shots to obtain a good signal-to-noise ratio. The chirp induced by the transmissive optics was corrected with a home-built Matlab code. The delay at which pump and probe arrive simultaneously on the sample (*i.e.* zero time) was determined from the point of maximum positive slope of the TA signal rise for each wavelength.

Time Dependent Density Functional Theory (TD-DFT): Optimized $PC_{70}BM$ molecule geometries were calculated by DFT on the B3LYP/6-31G(d,p) level. Single-point energy, TD-DFT calculations were carried out on optimized geometries. All calculations were carried out with the Gaussian 09 package.[24]

Supporting Information

Supporting Information is available from the Wiley Online Library or from the authors.

Acknowledgements

The research reported in this publication was supported by funding from King Abdullah University of Science and Technology (KAUST).

Received: ((will be filled in by the editorial staff))

Revised: ((will be filled in by the editorial staff))

Published online: ((will be filled in by the editorial staff))

5. References

[1] H. W. Kroto, J. R. Heath, S. C. O'Brien, R. F. Curl, R. E. Smalley, Nature 1985, 318, 162; I. Fraga Domínguez, A. Distler, L. Lüer, Advanced Energy Materials 2017, 7, 1601320; E. M. Speller, Materials Science and Technology 2017, 33, 924; P. Hudhomme, EPJ Photovolt. 2013, 4, 40401.
[2] T. Hahn, S. Tscheuschner, C. Saller, P. Strohriegl, P. Boregowda, T. Mukhopadhyay, S. Patil, D. Neher, H. Bässler, A. Köhler, The Journal of Physical Chemistry C 2016, 120, 25083.
[3] C. Keiderling, S. Dimitrov, J. R. Durrant, The Journal of Physical Chemistry C 2017, 121, 14470.
[4] P. C. Y. Chow, S. Albert-Seifried, S. Gélinas, R. H. Friend, Advanced Materials 2014, 26, 4851.
[5] S. Cook, H. Ohkita, Y. Kim, J. J. Benson-Smith, D. D. C. Bradley, J. R. Durrant, Chemical Physics Letters 2007, 445, 276.
[6] Y. Zou, R. J. Holmes, Advanced Energy Materials 2015, 5, 1500019.
[7] J. Jung, A. Stefaniuk-Grams, J. Ulanski, The Journal of Physical Chemistry C 2017, 121, 20650.
[8] A. Melianas, V. Pranculis, D. Spoltore, J. Benduhn, O. Inganäs, V. Gulbinas, K. Vandewal, M. Kemerink, Advanced Energy Materials 2017, 7, 1700888.
[9] G. F. Burkhard, E. T. Hoke, Z. M. Beiley, M. D. McGehee, The Journal of Physical Chemistry C 2012, 116, 26674.
[10] W. Li, H. Yu, J. Zhang, Y. Yao, C. Wu, X. Hou, The Journal of Physical Chemistry C 2014, 118, 11928; X. Xiao, J. D. Zimmerman, B. E. Lassiter, K. J. Bergemann, S. R. Forrest, Applied Physics Letters 2013, 102, 073302; X. Yan, B. Chu, W. Li, Z. Su, T. Zhang, F. Jin, B. Zhao, F. Zhang, D. Fan, Y. Gao, T. Tsuboi, J. Wang, H. Pi, J. Zhu, Organic Electronics 2013, 14, 1805.
[11] Y.-q. Zheng, W. J. P. Jr., T. Komino, C. Adachi, Applied Physics Letters 2013, 102, 153302; M. Zhang, H. Wang, H. Tian, Y. Geng, C. W. Tang, Advanced Materials 2011, 23, 4960; T. Zhuang, X.-F. Wang, T. Sano, Z. Hong, Y. Yang, J. Kido, Applied Physics Letters 2013, 103, 203301.
[12] W.-Y. Sit, F. D. Eisner, Y.-H. Lin, Y. Firdaus, A. Seitkhan, A. H. Balawi, F. Laquai, C. H. Burgess, M. A. McLachlan, G. Volonakis, F. Giustino, T. D. Anthopoulos, Advanced Science, 1700980.
[13] F. Yuliar, S. Akmaral, E. Flurin, S. Wai-Yu, K. Zhipeng, W. Nimer, B. A. H., Y. Emre, K. Safakath, L. Frédéric, A. T. D., Solar RRL, 0, 1800095.
[14] J. Gorenflot, A. Paulke, F. Piersimoni, J. Wolf, Z. Kan, F. Cruciani, A. E. Labban, D. Neher, P. M. Beaujuge, F. Laquai, Advanced Energy Materials, 1701678; M. A. Filatov, S. Karuthedath, P. M. Polestshuk, S. Callaghan, K. Flanagan, M. Telitchko, T. Wiesner, F. Laquai, M. O. Senge, Physical Chemistry Chemical Physics 2018; U. Schmidhammer, P. Jeunesse, G. Stresing, M. Mostafavi, Applied Spectroscopy 2014, 68, 1137; O. Alqahtani, M. Babics, J. Gorenflot, V. Savikhin, T. Ferron, A. H. Balawi, A. Paulke, Z. Kan, M. Pope, A. J. Clulow, J. Wolf, P. L. Burn, I. R. Gentle, D. Neher, M. F. Toney, F. Laquai, P. M. Beaujuge, B. A. Collins, Advanced Energy Materials, 0, 1702941; S. Karuthedath, A. Melianas, Z. Kan, V. Pranculis, M. Wohlfahrt, J. I. Khan, J. Gorenflot, Y. Xia, O. Inganas, V. Gulbinas, M. Kemerink, F. Laquai, Journal of Materials Chemistry A 2018.
[15] D. W. Gehrig, I. A. Howard, F. Laquai, The Journal of Physical Chemistry C 2015, 119, 13509.
[16] J. Jaumot, R. Gargallo, A. de Juan, R. Tauler, Chemometrics and Intelligent Laboratory Systems 2005, 76, 101; A. de Juan, J. Jaumot, R. Tauler, Analytical Methods 2014, 6, 4964; J. Jaumot, R. Gargallo, R. Tauler, Journal of Chemometrics 2004, 18, 327.
[17] A. Sperlich, M. Liedtke, J. Kern, H. Kraus, C. Deibel, S. Filippone, J. L. Delgado, N. Martín, V. Dyakonov, physica status solidi (RRL) – Rapid Research Letters 2011, 5, 128.

[18] D. R. Lawson, D. L. Feldhiem, C. A. Foss, P. K. Dorhout, C. M. Elliott, C. R. Martin, B. Parkinson, The Journal of Physical Chemistry 1992, 96, 7175.
[19] T. M. Clarke, C. Lungenschmied, J. Peet, N. Drolet, K. Sunahara, A. Furube, A. J. Mozer, Advanced Energy Materials 2013, 3, 1473.
[20] S. Kazaoui, N. Minami, Y. Tanabe, H. J. Byrne, A. Eilmes, P. Petelenz, Physical Review B 1998, 58, 7689.
[21] S. Karuthedath, T. Sauermann, H.-J. Egelhaaf, R. Wannemacher, C. J. Brabec, L. Luer, Journal of Materials Chemistry A 2015, 3, 3399.
[22] Y. W. Soon, H. Cho, J. Low, H. Bronstein, I. McCulloch, J. R. Durrant, Chemical Communications 2013, 49, 1291.
[23] J. R. Ochsmann, D. Chandran, D. W. Gehrig, H. Anwar, P. K. Madathil, K.-S. Lee, F. Laquai, Macromolecular Rapid Communications 2015, 36, 1122; I. A. Howard, R. Mauer, M. Meister, F. Laquai, Journal of the American Chemical Society 2010, 132, 14866.
[24] M. J. Frisch, G. W. Trucks, H. B. Schlegel, G. E. Scuseria, M. A. Robb, J. R. Cheeseman, G. Scalmani, V. Barone, G. A. Petersson, H. Nakatsuji, X. Li, M. Caricato, A. V. Marenich, J. Bloino, B. G. Janesko, R. Gomperts, B. Mennucci, H. P. Hratchian, J. V. Ortiz, A. F. Izmaylov, J. L. Sonnenberg, Williams, F. Ding, F. Lipparini, F. Egidi, J. Goings, B. Peng, A. Petrone, T. Henderson, D. Ranasinghe, V. G. Zakrzewski, J. Gao, N. Rega, G. Zheng, W. Liang, M. Hada, M. Ehara, K. Toyota, R. Fukuda, J. Hasegawa, M. Ishida, T. Nakajima, Y. Honda, O. Kitao, H. Nakai, T. Vreven, K. Throssell, J. A. Montgomery Jr., J. E. Peralta, F. Ogliaro, M. J. Bearpark, J. J. Heyd, E. N. Brothers, K. N. Kudin, V. N. Staroverov, T. A. Keith, R. Kobayashi, J. Normand, K. Raghavachari, A. P. Rendell, J. C. Burant, S. S. Iyengar, J. Tomasi, M. Cossi, J. M. Millam, M. Klene, C. Adamo, R. Cammi, J. W. Ochterski, R. L. Martin, K. Morokuma, O. Farkas, J. B. Foresman, D. J. Fox, Wallingford, CT 2016.